CALPHAD 36 (2012) 16-22

Critical Assessment: Martensite–Start Temperature for the $\gamma \rightarrow \varepsilon$ Transformation

H.-S. Yang*, J. H. Jang*, H. K. D. H. Bhadeshia*† and D. W. Suh*

*Graduate Institute of Ferrous Technology (GIFT)
Pohang University of Science and Technology (POSTECH)
Pohang 790-784, Republic of Korea

†University of Cambridge
Materials Science and Metallurgy
Pembroke Street, Cambridge CB2 3QZ, U. K.

Abstract

It is increasingly important in the context of high–manganese steels of the kind that lead to twinning–induced plasticity to be able to estimate the temperature at which ε–martensite forms when austenite is cooled. We find that the thermodynamic method used in similar calculations for α' martensite cannot in many cases be implemented because of apparently imprecise thermodynamic data, a conclusion partly validated using limited first–principles calculations. Alternative, empirical methods are also evaluated. The austenite grain size dependence of the martensite–start temperature has also been rationalised in terms of existing theory for α' martensite. Experiments have also been conducted to show that the problem in dealing with the ε–martensite does not lie in the precision with which the transformation can be measured using dilatometry.

Keywords: Martensite; thermodynamics; epsilon; start temperature; high Mn steels

1 Introduction

The basis for the calculation of the martensite–start (M_S) temperature was reviewed some time ago by Kaufman and Cohen [1]; martensite is triggered when the free energy change for transformation without a composition change ($\Delta G^{\gamma\alpha'}$) reaches a critical value ($\Delta G^{\gamma\alpha'}_{M_S}$), the magnitude of which is determined by stored energies and kinetic phenomena [2, 3]. Here γ refers to austenite and α' to body–centred cubic or body–centred tetragonal martensite. The method has been applied with some success to the $\gamma \rightarrow \alpha'$ transformation [4–12] and forms the basis of computer programs which take as inputs the thermodynamic parameters of the parent and product phases and output the

transformation–start temperature (for example, [13]). In this way, the incorporation of a previously excluded element on the M_S temperature simply requires an understanding of how this element alters the thermodynamic stabilities of the phases involved.

Iron in which the atoms are arranged on a hexagonal lattice is designated ε. Although this is not a common allotrope in alloyed iron at ambient pressure, it is gaining importance in low–carbon, often low density, structural steels containing unconventionally large concentrations of manganese [14–16]. It is also the basis of many iron–based shape memory alloys [17–19]. The ε therefore features in reversible martensitic transformations and in steels where its transformation plasticity is exploited. It is important therefore, in the process of alloy design and optimisation, to be able to calculate its martensite–start temperature, at least as a function of the chemical composition.

The last attempt at dealing with this issue was by Dogan and Ozer [20] who derived an empirical equation using linear regression analysis on some 17 iron–based alloys which undergo the $\gamma \rightarrow \epsilon$ martensitic transformation as follows:

$$M_S/\mathrm{K} = 246 - 5.8w_{\mathrm{Mn}} + 38.5w_{\mathrm{Si}} - 61.5w_{\mathrm{Cr}} - 5.1w_{\mathrm{Ni}} + 138w_{\mathrm{Ce}} - 146w_{\mathrm{Ti}} - 396w_{\mathrm{N}} \quad (1)$$

where w represents the weight percent of the element identified in the subscript. The equation was derived for the concentration ranges 13.0–31.5Mn, 4.7–7.0Si, 0–11.6Cr, 0–6.8Ni wt%; Ce, Ti and N were each present in single alloys with values of 0.3, 0.6 and 0.3 wt% respectively. Standard errors were not quoted but the deviation from a fit to this equation were typically less than $\pm 20^\circ$C.

Dogan and Ozer also considered the use of thermodynamics as described above; however, neither the origin of the thermodynamic data nor the calculations of M_S temperatures were presented in the paper, so it is not clear what was achieved. The purpose of the present work was to take a fresh look at this problem given the much larger availability of data due to the increased modern interest in low density and TRIP (transformation induced plasticity) steels based on the ε phase. To achieve this we have used a variety of empirical, thermodynamic and first–principles techniques.

2 Data

A search of the literature revealed a large number of sources of data [20–78] which yielded some 328 combinations of chemical composition and martensite–start temperatures. The properties of the data are summarised in Table 1, and a spreadsheet containing the full details is available on [79]. The elements included C, Mn, Ni, Cr, Al, Si, Mo, Co, Cu, Nb, Ti, V and W.

The data were subjected to multiple regression analysis to yield the following relationship which has a standard error of ± 26 K and a correlation coefficient of 0.9:

$$\begin{aligned} M_S/\mathrm{K} \;=\; & 576 \pm 8 - (489 \pm 31)w_{\mathrm{C}} - (9.1 \pm 0.4)w_{\mathrm{Mn}} - (17.6 \pm 2)w_{\mathrm{Ni}} - (9.2 \pm 1)w_{\mathrm{Cr}} \\ & + (21.3 \pm 2)w_{\mathrm{Al}} + (4.1 \pm 1)w_{\mathrm{Si}} - (19.4 \pm 5)w_{\mathrm{Mo}} - (1 \pm 1)w_{\mathrm{Co}} - (41.3 \pm 6)w_{\mathrm{Cu}} \\ & - (50 \pm 18)w_{\mathrm{Nb}} - (86 \pm 12)w_{\mathrm{Ti}} - (34 \pm 10)w_{\mathrm{V}} - (13 \pm 5)w_{\mathrm{W}} \end{aligned} \quad (2)$$

The extent of the fit is illustrated in Fig. 1 and forms a rough method of estimating the martensite–start temperature but the linear relationship and the implied lack of dependences between the

independent variables clearly cannot be justified. These particular issues are tackled later in the text when describing the neural network method, but a more fundamental approach would involve calculations based on phase stabilities which we address next.

3 Thermodynamic Calculations

By analogy with the transformation of austenite into α' martensite described in the introduction, the martensite–start temperature for ε–martensite corresponds to that at which the driving force $\Delta G^{\gamma\varepsilon}$ achieves a critical value $\Delta G^{\gamma\varepsilon}_{M_S}$. Values of the driving force can in principle be calculated using standard thermodynamic databases in combination with programs such as ThermoCalc or MTDATA. In the present work we used the TCFE6 database and ThermoCalc to produce the results illustrated in Fig. 2, which shows $\Delta G^{\gamma\varepsilon}_{M_S}$ as a function of the measured transformation–start temperatures obtained from the literature. The results are worrying in two respects; first, that the driving force for a large number of alloys is positive, *i.e.,* it is thermodynamically impossible for ε to form even though it is actually observed, and second, even when $\Delta G^{\gamma\varepsilon}_{M_S}$ is negative, its magnitude is in many cases very small and possibly insufficient to account for the strain energy of transformation.

There are two ways in which these results might be understood. The first is that the experimental measurements of M_S temperatures are faulty, but a detailed examination of the original sources of information indicated that any error in M_S is much smaller than required to explain the sign and magnitude of the free energy change in cases where $\Delta G^{\gamma\varepsilon}_{M_S} \gg 0$. Nevertheless, we discuss later in this paper, our own experimental data designed to assess experimental error.

The second and more likely explanation is that the database which forms the basis of the thermodynamic calculations described in section 3 is insufficiently populated to represent ε–martensite in concentrated alloys and at the relatively low temperatures involved. First principles calculations based on electron theory can be used to check this second explanation, but the calculations are expensive to conduct so a particular alloy which indicated a large positive $\Delta G^{\gamma\epsilon} = G^{\varepsilon} - G^{\gamma}$ in spite of the observation of martensite was selected for study.

The conventional unit cells of austenite (FCC) and ε (HCP) can both be represented by the stacking of layers of close–packed planes, with each layer containing 4 atoms with a total of 24 atoms, and hence six layers, with both phases treated as being non–magnetic. The lattice parameters (a, c) of the conventional hexagonal unit cell is then determined as $a = \sqrt{2}a_\gamma$ and $c = 2\sqrt{3}a_\gamma$. The lattice parameter of austenite is applied as $a_\gamma = 3.59$Å[80]. The only difference between the FCC and HCP forms is then the stacking sequence which is ABCABC and ABABAB, respectively. The alloy composition is created by an appropriate substitution of Fe atoms with five Mn, two Si and two Cr atoms, Fig 3.

The Kohn-Sham equation was solved self-consistently in terms of the total energy all-electron full-potential linearised augmented plane-wave method [81, 82] by using the generalised gradient approximation for the exchange-correlation potential. The integrations over the three dimensional Brillouin zone (3D-BZ) were calculated by the tetrahedron method over a $7 \times 7 \times 5$ Monkhorst-Pack mesh [83], which corresponds to 123 k-points inside the irreducible wedge of 3D-BZ. The degree of

precision was obtained by considering a plane-wave cutoff up to 21 Ry, which corresponds to about 3245 linearised augmented plane-waves per each k-point and spin. The wave functions, the charge densities, and the potential were expanded with $l < 8$ lattice harmonics inside each muffin-tin sphere with a radius of 2.20 a.u. for Fe,Mn,Si and Cr. The density and potential in the interstitial region were depicted by using a star-function cutoff at 340 Ry. Self-consistency was assumed when the root-mean-square distances between the input and output total charges were not more than 2.0×10^{-3} electrons/a.u.^{3} The sphere radii and K_{max} within the whole lattice spacing range were kept constant, to keep the same degree of convergence for all the lattice constants studied.

The transformation energies at 0 K and zero pressure were calculated to give $\Delta G_{\gamma\varepsilon}$ as $-5.57\,\mathrm{kJ\ mol^{-1}}$ and $-3.49\,\mathrm{kJ\ mol^{-1}}$ for the transformation in pure iron and 15Fe-5Mn-2Si-2Cr alloy respectively, where the alloy composition is expressed in terms of the number of atoms out of a total of 24 atoms. The value for pure iron is remarkably consistent with the $-5.45\,\mathrm{kJ\ mol^{-1}}$ reported in [84] for one atomsphere of pressure and 0 K. based on a thermodynamic assessment. This calculation proves the need for better thermodynamic data for use in software such as Thermocalc or MTDATA. It is our intention in the future to undertake a major programme of first principles calculations, including lattice parameter calculations (as opposed to the fixed parameters assumed here) in order to assess and enhance the thermodynamic database for the ε phase.

Given the difficulties with the thermodynamic data, the best that can be done is focus on those alloys where the critical driving force $\Delta G^{\gamma\varepsilon}_{M_S} < 0$ (i.e., a reduction in free energy). Given the availability of data from binary Fe–Mn alloys with large differences in the manganese concentrations, the dependence of $\Delta G^{\gamma\varepsilon}_{M_S}$ on Mn has been derived as illustrated in Fig. 4a. Calculations carried out to estimate M_S assuming that all other solutes influence only $\Delta G^{\gamma\varepsilon}$ are shown in Fig. 4b. Note that we do not understand the functional dependence illustrated in Fig. 4a, and that the accuracy of the predictions illustrated in Fig. 4b is not impressive even when the analysis is limited to those cases where the transformation is accompanied by a reduction in free energy.

4 Experiments

The purpose of the work presented here was to check the level of experimental error expected in measuring the start temperature for ε, given that the volume change of transformation might in some cases be rather small [85, 86]. A set of six alloys showing a variation in manganese and silicon concentrations, was prepared as 300 g melts, which were cast and vacuum sealed. They were then homogenised for 2 days at 1473 K, after which their chemical compositions were measured as listed in Table 2. Cylindrical dilatometer samples 5 mm diameter and 10 mm long were machined and studied using a BAHR DIL805 dilatometer. The samples were heated at $2\,\mathrm{K\,s^{-1}}$ in a vacuum to 873 K for 1min, and then quenched at $10\,\mathrm{K\,s^{-1}}$ using argon gas to room temperature.

The results of dilatometric experiments are presented in Fig. 5. A method exists which enables such data to be interpreted objectively, so that any user analysing the same data should obtain an identical transformation–start temperature [87]. The technique defines the first onset of transformation to be that at which a critical strain is achieved relative to the thermal contraction of the parent phase. In the present work the critical strain has been taken as 1/100 of the total transformation strain determined at ambient temperature for the 16Mn 0Si alloy, equal to -4.6×10^{-5}.

Note that although this small offset should be greater than the noise in the data, it is an arbitrary but reproducible value which is used for all the alloys. It is akin to the arbitrary, small strain used in defining the proof strength in a gradually yielding tensile test. Optical metallography was used to confirm the existence of ϵ–martensite and two representative examples are presented in Fig. 6.

Using this method, it is clear from Table 2 that with one exception where the volume change on transformation is rather small, the uncertainties in the determination of martensite–start temperatures are small and cannot explain the major discrepancies found in the $\Delta G_{\gamma\varepsilon}$ values calculated using existing thermodynamic databases.

5 Neural Network

The most general method of regression analysis is the neural network, because it is able to capture non–linear and non–periodic functions of immense complexity without bias on the form of the function. Comprehensive details of this method have been described elsewhere [88–91] and hence are not reproduced here except when the information is necessary to reproduce the work.

To create a network which is not too simple, nor so complex that it models the noise in the information, the data were partitioned at random into approximately equal training and test sets. The former was used to create the models and the latter to test their ability to generalise. Once the appropriate level of complexity is achieved, the entire data can be used to retrain the network without changing its configuration. The results, having gone through these procedures, are illustrated in Fig. 7 and show that the optimised network performs well on the unseen test data.

We now show an example to illustrate the non–linear capability of the neural network, which is consistent with expectations from physical metallurgy but would not be captured by a linear regression equation. The Néel temperature T_N of austenite is raised almost linearly by the addition of manganese [38] and this has an enhanced effect on suppressing the ε martensite–start temperature if the latter is below T_N [92]. That this phenomenon is correctly represented by the neural network is illustrated in Fig. 8.

6 Austenite Grain Size Effect

It has been shown recently [93] that the dependence of M_S on the austenite grain size during the $\gamma \rightarrow \alpha'$ transformation can be explained quantitatively on the basis of Fisher's original suggestion [94] that the number of plates per unit volume needed in order to obtain a detectable fraction of martensite increases as the austenite grain volume (V_γ) decreases, because the plate size and hence the volume transformed per plate is reduced with V_γ. This leads to an expression [93]:

$$M_S^o - T = \frac{1}{b} \ln \left[\frac{1}{aV_\gamma} \left\{ \exp\left(-\frac{\ln(1-f)}{m} \right) - 1 \right\} + 1 \right] \tag{3}$$

where $M_S \rightarrow M_S^o$ as $V_\gamma \rightarrow \infty$, and f is the fraction of martensite, with the volume measured in mm^3 the term a can be set to unity, m is the aspect ratio of martensite plates, and b is a constant. This

relationship enables the amount of martensite to be calculated as a function of undercooling below M_S with the latter defined by the undercooling needed to achieve a detectable fraction f_{M_S}. When the temperature T is sufficiently below M_S^o the equation reduces to the classical Koistinen and Marburger relation [95] which is independent of grain size and expressed here in the terminology of equation 3:

$$\ln\{1-f\} = -m \ln V_\gamma - mb(M_S^o - T) \tag{4}$$

where Koistinen and Marburger obtained $mb = 0.011\,\mathrm{K}^{-1}$ for the $\gamma \rightarrow \alpha'$ transformation. The two relationships in fact only differ in the narrow temperature range at the beginning of transformation.

There exist three sets of experiments where ε–martensite has been studied as a function of the austenite grain size [29, 39, 62]. Fig. 9a shows that all three sets of data can be used to derive $b = 0.33$, and taking the aspect ratio of ε as $m = 0.03$ [39], $mb = 0.01\,\mathrm{K}^{-1}$, a value which is remarkably similar to the original due to Koistinen and Marburger for α' martensite. This may well be a coincidence but the fact that these values are not dramatically different nevertheless inspires confidence in the analysis. The values of M_S^o are also obtained from the intercepts on the vertical axes of Fig. 9a. The final results are plotted in Fig. 9b, showing that all the data can be rationalised in terms of equation 3. Jiang *et al.* [62] in their work concluded that there is no grain size dependence of M_S for ε, but Fig. 9b shows that this is because the grain size was not varied sufficiently in their experiments.

7 Conclusions

The thermodynamic method used so successfully in predicting the M_S temperature for the $\gamma \rightarrow \alpha'$ transformation cannot be implemented fully for ε because of the availability of thermodynamic data. A reasonable assumption can be made that it is the dataset for ε which is lacking since the γ phase is well characterised. This is partly supported by a limited calculation done using first principles, but to do this generally is an expensive option and the focus perhaps needs to be on specific cases of technological interest. A limited number of experiments on six combinations of manganese and silicon supports the conclusion that the thermodynamic data are wanting, and the problem does not lie in potential inaccuracies in the measurement of martensite–start temperatures.

A linear regression equation has been derived based on a large experimental dataset accumulated from the published literature, as a rough method for estimating the $\gamma \rightarrow \varepsilon$ martensite–start temperatures. This is unable to capture the non–linear effects apparent in the experimental data, for example the dependence on the manganese concentration. Therefore, a corresponding neural network model has also been created, which should be a better tool than the linear method.

It has been demonstrated that the austenite grain size dependence of the start–temperature for ε martensite can be rationalised in terms of existing theory which is based on the fact that the minimum detectable quantity of transformation, which defines M_S, is a function of the grain size.

The neural network models, thermodynamic calculations and the full set of compiled data can be downloaded from [79].

Acknowledgments

We acknowledge Professor Nack Joon Kim for the provision of laboratory facilities at GIFT, and support from POSCO through the Steel Innovation Programme. The authors are also grateful for support from the World Class University Programme of the National Research Foundation of Korea, Ministry of Education, Science and Technology, project number R32–2008–000–10147–0.

References

[1] L. Kaufman, M. Cohen: Progress in Metal Physics 7 (1958) 165–246.

[2] G. B. Olson, M. Cohen: Metallurgical Transactions A 7A (1976) 1897–1923.

[3] J. W. Christian: Thermodynamics and kinetics of martensite: in: G. B. Olson, M. Cohen (Eds.), International Conference on Martensitic Transformations ICOMAT '79: 1979: pp. 220–234.

[4] L. Kaufman, S. V. Radcliffe, M. Cohen: Thermodynamics of the bainite reaction: in: V. F. Zackay, H. I. Aaronson (Eds.), Decomposition of Austenite by Diffusional Processes: Interscience, New York, USA, 1962: pp. 313–352.

[5] Y. Imai, M. Izumiyama, M. Tsuchiya: Scientific Reports: Research Institute of Tohoku University A17 (1965) 173–192.

[6] T. Bell, W. S. Owen: Trans. Metall. Soc. AIME 239 (1967) 1940–1949.

[7] H. K. D. H. Bhadeshia: Metal Science 15 (1981) 175–177.

[8] H. K. D. H. Bhadeshia: Metal Science 15 (1981) 178–180.

[9] H. Chang, T. Y. Hsu: Acta Metallurgica 34 (1986) 333–338.

[10] G. Ghosh, G. B. Olson: Acta Metallurgica and Materialia 42 (1994) 3361–3370.

[11] J. Wang, P. J. van der Wolk, S. van der Zwaag: Materials Transactions JIM 41 (2000) 769–776.

[12] G. Ghosh, G. B. Olson: Journal of Phase Equilibria 22 (2001) 199–207.

[13] U. of Cambridge, NPL: Materials Algorithms Project, www.msm.cam.ac.uk/map/mapmain.html

[14] O. Grässel, L. Kruger, G. Frommeyer, L. W. Meyer: International Journal of Plasticity 16 (2000) 1391–1409.

[15] G. Frommeyer, U. Brüx, P. Neumann: ISIJ International 43 (2003) 438–446.

[16] D. Embury, O. Bouaziz: Annual Reviews in Materials Science 40 (2010) 213–241.

[17] A. Sato, E. Shishima, Y. Yamaji, T. Mori: Acta Metallurgica 32 (1984) 539–547.

[18] J. Li, C. M. Wayman: Materials Characterization 32 (1994) 215–227.

[19] Y. Tomota, T. Maki: Materials Science Forum 327–328 (2000) 191–198.

[20] A. Dogan, T. Ozer: Canadian Metallurgical Quarterly 44 (2005) 555–561.

[21] Q. X. Dai, X. N. Cheng, Y. T. Zhao, X. M. Luo, Z. Z. Yuan: Materials Characterization 52 (2004) 349–354.

[22] S. H. Baik, J. C. Kim, K. K. Jee, M. C. Shin, C. S. Choi: ISIJ International 37 (1997) 519–522.

[23] M. Sade, K. Halter, E. Hornbogen: Journal of Materials Science Letters 9 (1990) 112–115.

[24] T. Liu, Z. T. Zhao, R. Z. Ma: Phase Transitions 69 (1999) 425–428.

[25] N. van Caenegem, L. Duprez, K. Verbeken, D. Segers, Y. Houbaert: Materials Science & Engineering A 481–482 (2008) 183–189.

[26] S. Takaki, T. Furuya, Y. Tokunaga: ISIJ International 30 (1990) 632–638.

[27] Y. K. Lee, C. S. Choi: Metallurgical & Materials Transactions A 31 (2000) 355–360.

[28] Y. Tomota, M. Stum, J. W. Morris Jr.: Metallurgical Transactions A 17 (1986) 537–547.

[29] J. H. Jun, C. S. Choi: Materials Science & Engineering A 257 (1998) 535–556.

[30] Y. Tomota, Y. Morioka, W. Nakagawara: Acta Materialia 46 (1998) 1419–1426.

[31] Y. K. Lee, J. H. Jun, C. S. Choi: Scripta Materialia 35 (1996) 825–830.

[32] Y. K. Lee, J. H. Jun, C. S. Choi: ISIJ International 37 (1997) 1023–1030.

[33] J.-H. Jun, D.-K. Kong, C.-S. Choi: Materials Research Bulletin 33 (1998) 1419–1425.

[34] J. H. Jun, C. S. Choi: Scripta Materialia 38 (1998) 543–549.

[35] J. H. Jun, C. S. Choi: Materials Science & Engineering A 252 (1998) 133–138.

[36] S. Cotes, M. Sade, A. F. Guillermet: Metallurgical and Materials Transactions A 26 (1995) 1957–1969.

[37] J. T. Lenkkeri, J. Levoska: Philosophical Magazine A 48 (1983) 749–758.

[38] H. Umebayashi, Y. Ishikawa: Journal of the Physical Society of Japan 21 (1966) 1281–1294.

[39] S. Takaki, H. Nakatsu, T. Tokunaga: Materials Transactions JIM 34 (1993) 489–495.

[40] S. Cotes, A. F. Guillermet, M. Sade: Journal of Alloys and Compounds 278 (1998) 231–238.

[41] I. Y. Georgiyeva, N. A. Sorokina, V. I. Gal'tsova: Physics of Metals and Metallography 49 (1981) 178–181.

[42] K. Ishida, T. Nishizawa: Transactions of the Japan Institute of Metals 15 (1974) 225–231.

[43] A. P. Gulyaev, T. F. Volynova, I. Y. Georgiyeva: Metals Science and Heat Treatment 20 (1978) 179–182.

[44] A. R. Troiano, F. T. McGuire: Trans. ASM 31 (1943) 340–364.

[45] I. N. Bogachev, L. S. Malinov: Physics of Metals and Metallography 14 (1962) 828–833.

[46] I. N. Bogachev, V. F. Yegolayev, G. Y. Zvigintseva, L. V. Zhuravel: Physics of Metals and Metallography 28 (1968) 885–888.

[47] M. Eskil, E. Kanaca: Computational Materials Science 43 (2008) 774–784.

[48] A. Druker, A. Baruj, J. Malarria: Materials Characterization 61 (2010) 603–612.

[49] C. H. Yang, H. C. Lin, K. M. Lin: Materials Science & Engineering A 518 (2009) 139–143.

[50] K. Tsuzaki, S. Fukasaku, Y. Tomota, T. Maki: Trans. JIM 32 (1991) 222–228.

[51] H. Otsuka, H. Yamada, T. Maruyama, H. Tanahashi, S. Matsuda, M. Murakami: ISIJ International 30 (1990) 674–679.

[52] M. Fujita, I. Uchiyama: Tetsu–to–Hagane 60 (1974) 525–539.

[53] A. A. H. Hamers, C. M. Wayman: Scripta Metallurgica and Materialia 25 (1991) 2723–2728.

[54] P. Donner, E. Hornbogen, M. Sade: Journal of Materials Science 8 (1989) 37–40.

[55] A. Baruj, S. Cotes, M. Sade, A. F. Guillermet: Journal de Physique Colloque 5 (1995) C8 373–378.

[56] M. Acet, T. Schneider, B. Gehrmann, E. F. Wassermann: Journal de Physique Colloque 5 (1995) C8 379–384.

[57] K. K. Jee, W. Y. Jang, S. H. Baik, M. C. Shin, C. S. Choi: Journal de Physique Colloque 5 (1995) C8 385–390.

[58] T. Bouraoui, A. van Neste, B. Dubois: Journal de Physique Colloque 5 (1995) C8 403–408.

[59] D. P. Dunne, H. Li: Journal de Physique Colloque 5 (1995) C8 415–420.

[60] Y. Tomota, K. Yamaguchi: Journal de Physique Colloque 5 (1995) C8 421–426.

[61] M. Andersson, J. A. gren: Journal de Physique Colloque 5 (1995) C8 457–462.

[62] B. H. Jiang, X. Qi, W. Zhou, T. Y. Hsu: Scripta Materialia 34 (1996) 771–773.

[63] L. J. Rong, D. H. Ping, Y. Y. Li, C. X. Shi: Scripta Materialia 32 (1995) 1905–1909.

[64] S. Chen, C. Y. Chung, C. Yan, T. Y. Hsu: Materials Science & Engineering A 264 (1999) 262–268.

[65] H. Li, D. Dunne, N. Kennon: Materials Science & Engineering A 273–275 (1999) 517–523.

[66] X. Wu, T. Y. Hsu: Materials Characterization 45 (2000) 137–142.

[67] Y. Wen, N. Li, M. Tu: Scripta Materialia 44 (2001) 1113–1116.

[68] W. Zhou, B. Jiang, X. Qi, T. Y. Hsu: Scripta Materialia 39 (1998) 1483–1487.

[69] Y. H. Wen, M. Yan, N. Li: Scripta Materialia 50 (2004) 441–444.

[70] Z. Wang, J. Zhu: Wear 256 (2004) 66–72.

[71] B. C. Maji, M. Krishnan: Scripta Materialia 48 (2003) 71–77.

[72] Y. S. Zhang, X. Lu, X. Tian, Z. Qin: Materials Science & Engineering A 334 (2002) 19–27.

[73] Y. H. Wen, W. L. Xie, D. Li: Materials Science & Engineering A 457 (2007) 334–337.

[74] V. G. Gavriljuk, V. V. Bliznuk, B. D. Shanina, S. P. Kolesnik: Materials Science & Engineering A 406 (2005) 1–10.

[75] K. Yamaguchi, Y. Morioka, Y. Tomota: Scripta Materialia 35 (1996) 1147–1152.

[76] C. L. Li, D. J. Cheng, Z. H. Jin: Scripta Materialia 35 (1996) 1147–1152.

[77] J. H. Yang, H. Chen, C. M. Wayman: Metallurgical Transactions A 23 (1992) 1431–1437.

[78] Y. Tomota, W. Nakagawara, K. Tsuzaki, T. Maki: Scripta Materialia 26 (1992) 1571–1574.

[79] H. S. Yang: Data for epsilon martensite–start temperatures in steels, http://www.msm.cam.ac.uk/map/steel/programs/epsilon.Ms.html and http://cml.postech.ac.kr/2011/epsilon.zip (2011).

[80] A. Lambert-Perlade: Rupture par clivage de microstructures d'aciers bainitiques obtenues en conditions de soudage: Ph.D. thesis: Ecole de Mines de Paris: Paris, France (2001).

[81] E. Wimmer, H. Karkauer, M. Weinert, A. J. Freeman: Physical Review B 24 (1981) 864–875.

[82] M. Weinert, E. Wimmer, A. J. Freeman: Physical Review B 26 (1982) 4571–4578.

[83] H. J. Monkhorst, J. D. Pack: Physical Review B 13 (1976) 3865–3868.

[84] L. Kaufman, E. V. Clougherty, R. J. Weiss: Acta Metallurgica 11 (1963) 323–335.

[85] J. W. Brooks, M. H. Loretto, R. E. Smallman: Acta Metallurgica 27 (1979) 1829–1838.

[86] J. W. Brooks, M. H. Loretto, R. E. Smallman: Acta Metallurgica 27 (1979) 1839–1847.

[87] H.-S. Yang, H. K. D. H. Bhadeshia: Materials Science and Technology 23 (2007) 556–560.

[88] D. J. C. MacKay: Neural Computation 4 (1992) 448–472.

[89] D. J. C. MacKay: Neural Computation 4 (1992) 415–447.

[90] H. K. D. H. Bhadeshia: Statistical Analysis and Data Mining 1 (2009) 296–305.

[91] H. K. D. H. Bhadeshia, R. C. Dimitriu, S. Forsik, J. H. Pak, J. H. Ryu: Materials Science and Technology 25 (2009) 504–510.

[92] M. Palumbo: CALPHAD 32 (2008) 693–708.

[93] H. S. Yang, H. K. D. H. Bhadeshia: Scripta Materialia 60 (2009) 493–495.

[94] J. C. Fisher, J. H. Hollomon, D. Turnbull: Metals Transactions 185 (1949) 691–700.

[95] D. P. Koistinen, R. E. Marburger: Acta Metallurgica 7 (1959) 59–60.

Table 1: Dataset statistics, rounded off to significant figures after the decimal point, for a total of 328 separate measurements as described in the text. The concentrations of solutes are in wt%.

	Minimum	Maximum	Average	Standard deviation
C	0	0.35	0.02	0.05
Mn	11.2	35.9	22.2	6
Ni	0	6.8	0.47	1.5
Cr	0	13.7	1.5	3.2
Al	0	5	0.16	0.8
Si	0	7.1	2.1	2.5
Mo	0	4.46	0.03	0.3
Co	0	8	0.29	1.2
Cu	0	3.1	0.03	0.25
Nb	0	1.21	0.01	0.08
Ti	0	1.72	0.01	0.12
V	0	2.2	0.01	0.15
W	0	4.48	0.03	0.31
M_S / K	167	467	352	60

Table 2: Alloy compositions and measured M_S temperatures

Alloy designation	Mn / wt%	Si / wt%	M_S / K
16Mn 0 Si	15.8	0.0	410 ± 3
16Mn 3 Si	15.6	2.7	437 ± 7
16Mn 6 Si	16.0	5.4	422 ± 1
25Mn 0 Si	24.8	0.1	< 293
25Mn 3 Si	25.3	2.8	343 ± 2
25Mn 6 Si	25.0	5.2	441 ± 1

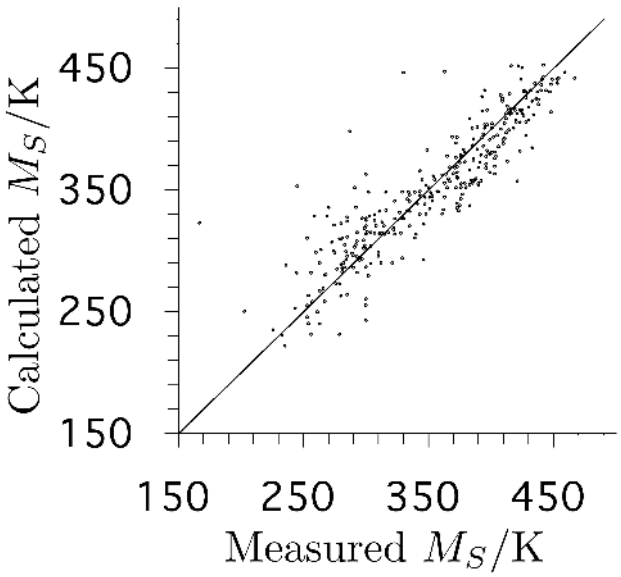

Figure 1: The ε–martensite M_S temperatures estimated using equation 2, versus measured values.

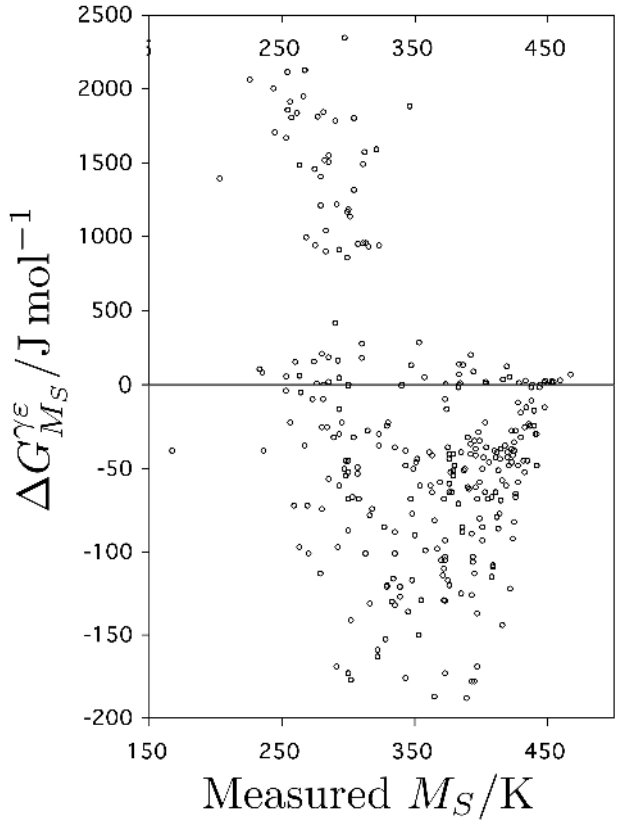

Figure 2: The calculated free energy change accompanying the formation of ε–martensite at the measured M_S temperature. Notice that the scales above and below the abscissa are different. The samples for which $\Delta G^{\gamma\varepsilon}_{M_S} \geq 0$ are generally those which have large total solute concentrations, for example, Fe–26Mn–5Cr–6Si wt%.

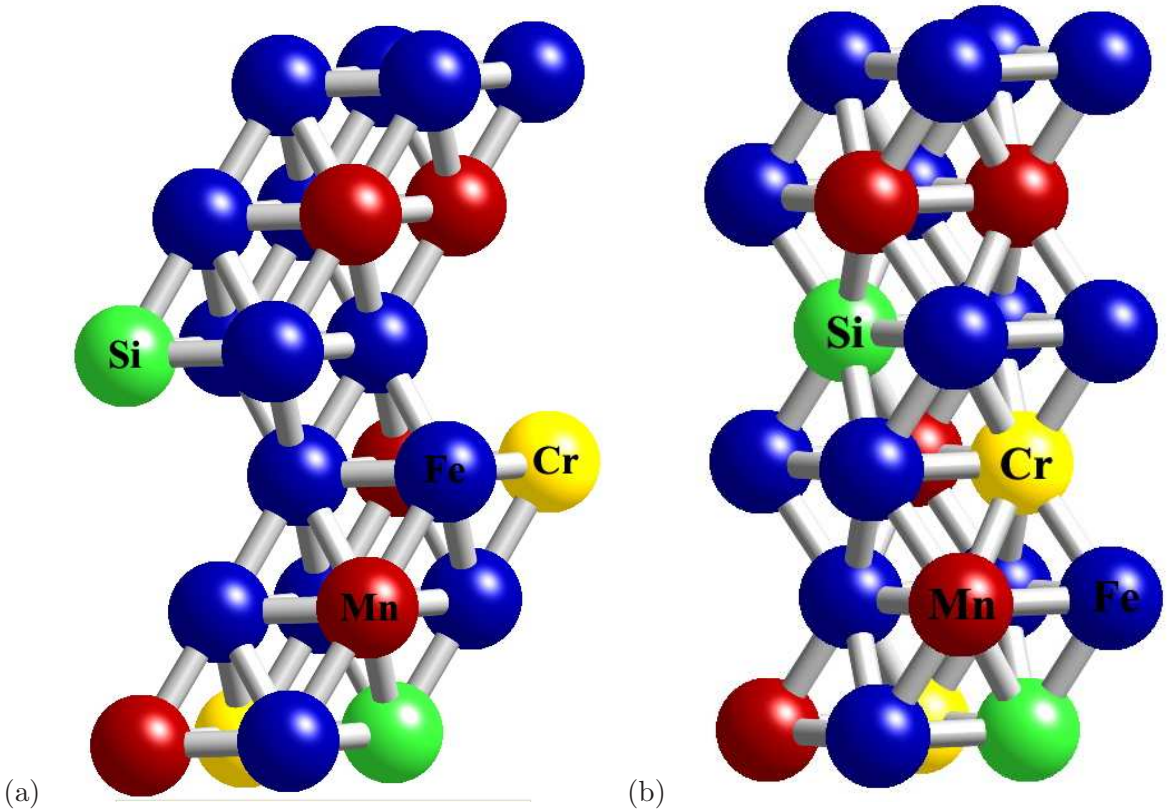

(a) (b)

Figure 3: The supercells used in the first–principles calculations.

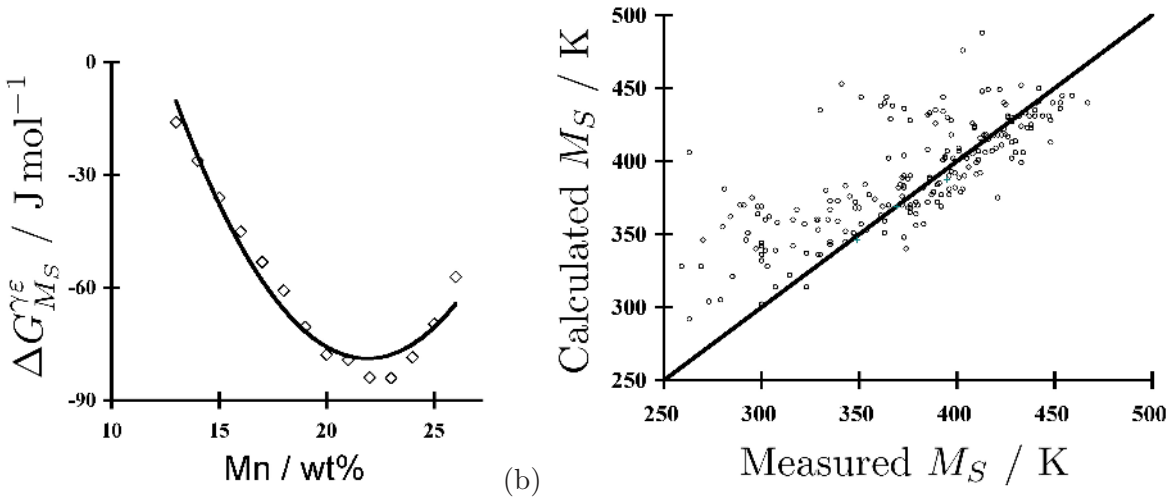

(a) (b)

Figure 4: Thermodynamic method applied only to those alloys for which $\Delta G^{\gamma\varepsilon}_{M_S} < 0$ using current thermodynamic databases. (a) Dependence of $\Delta G^{\gamma\varepsilon}_{M_S}$ on the manganese concentration. (b) An illustration of the accuracy with which predictions can be made assuming that the critical driving force at M_S varies only with the Mn concentration.

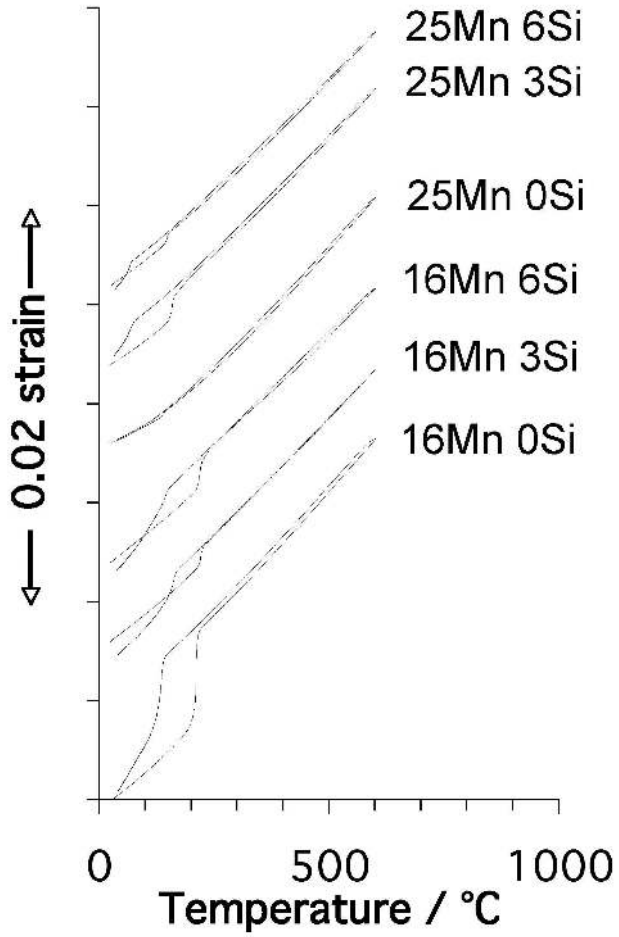

Figure 5: Heating and cooling dilatometric data for all of the experimental alloys. Note that there is a contraction when ε–martensite forms from austenite. The data here are presented with a compressed vertical axis for the sake of brevity, but the full, high–resolution set is available on [79].

(a) 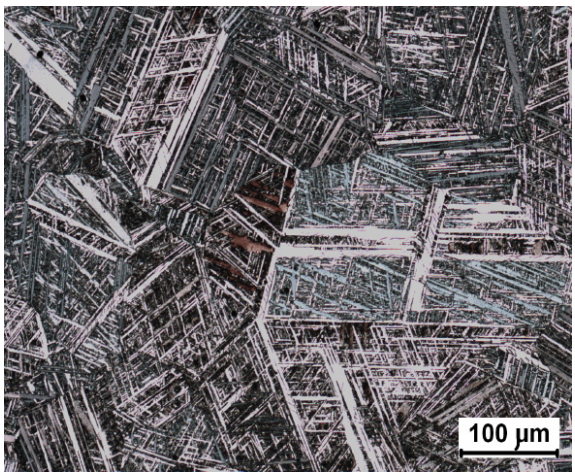

(b) 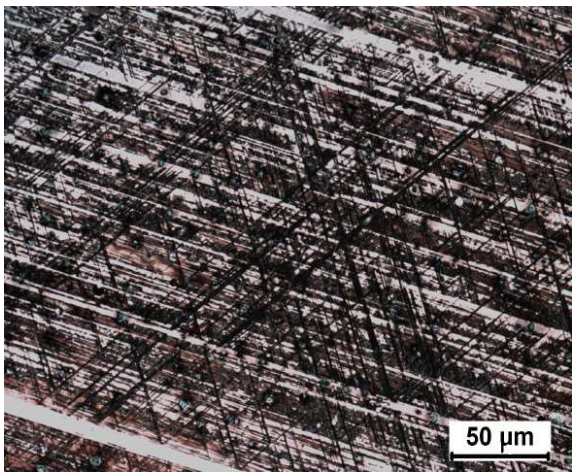

Figure 6: Optical micrographs showing ε martensite. (a) 16Mn 0Si alloy. (b) 25Mn 3Si alloy.

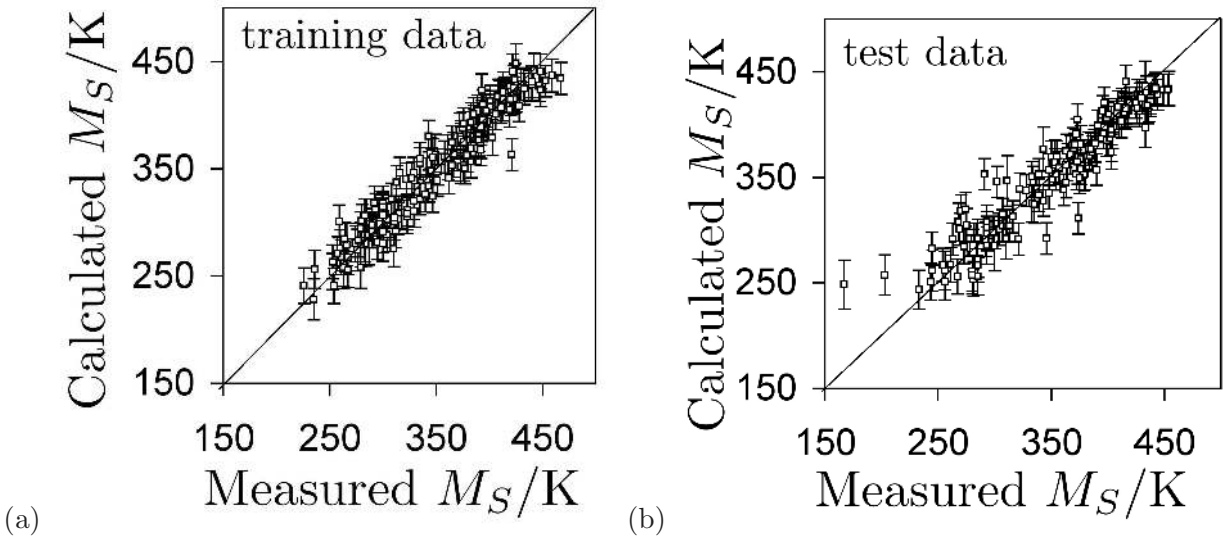

(a) (b)

Figure 7: Illustration of the fit achieved with a neural network of optimum complexity. The error bars represent $\pm 1\sigma$ modelling uncertainty. (a) Data used to create the network. (b) Unseen data used to test the network.

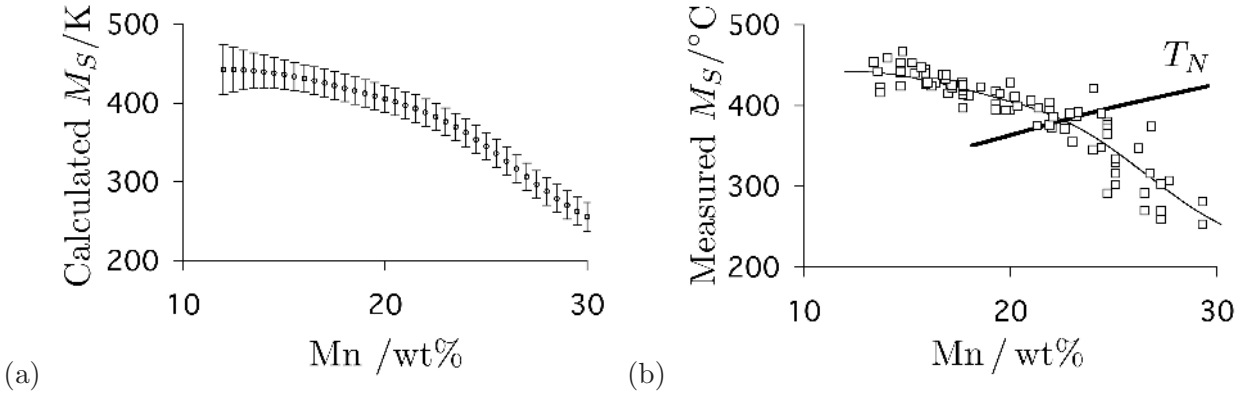

(a) (b)

Figure 8: Variation in the martensite–start temperature in Fe–Mn alloys as a function of the manganese concentration. (a) Calculated using neural network. (b) Measured values from published work, together with the calculated curve from (a). The Néel temperature (T_N) data are from [38].

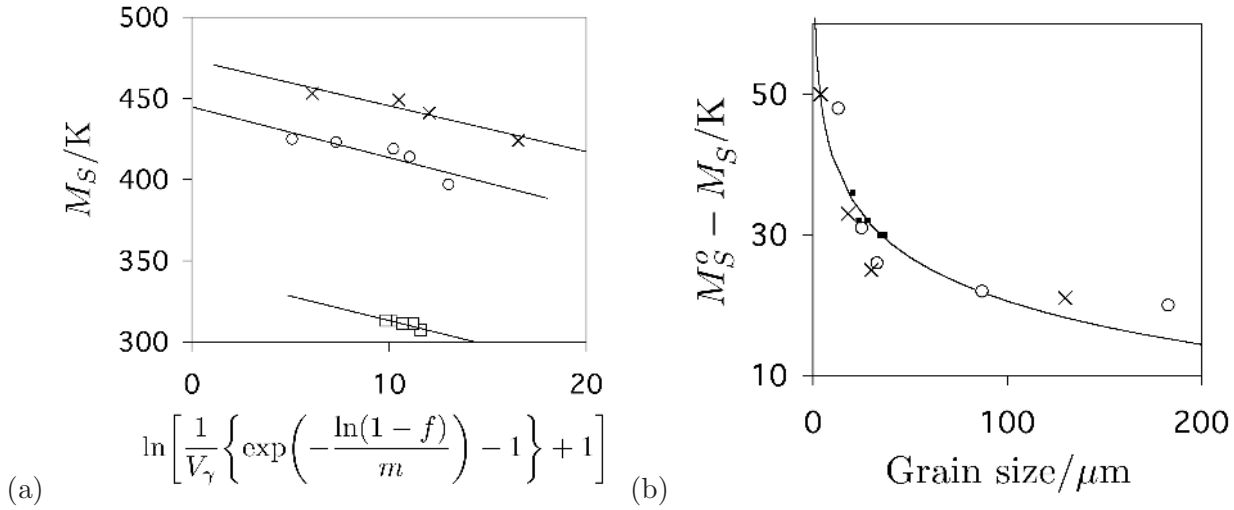

Figure 9: Analysis of the austenite grain size dependence of M_S for ε–martensite. The circles, crosses and squares are data from [29], [39] and [62] respectively. (a) Linear regression to derive b and M_S^o. (b) Comparison between measured data and curve calculated using equation 3.